Coherence effects in scattering order expansion of light by atomic clouds

Mohamed-Taha Rouabah,[1,2] Marina Samoylova,[3] Romain Bachelard,[4] Philippe W. Courteille,[4] Robin Kaiser,[1] and Nicola Piovella[3,*]

[1]*Université de Nice Sophia Antipolis, CNRS, Institut Non-Linéaire de Nice, UMR 7335, F-06560 Valbonne, France*
[2]*Laboratoire de Physique Mathematique et Physique Subatomique, Université Constantine 1, Route Ain El Bey, 25017 Constantine, Algeria*
[3]*Dipartimento di Fisica, Università degli Studi di Milano, Via Celoria 16, I-20133 Milano, Italy*
[4]*Instituto de Física de São Carlos, Universidade de São Paulo, 13560-970 São Carlos, SP, Brazil*
**Corresponding author: nicola.piovella@unimi.it*

Received January 21, 2014; revised March 11, 2014; accepted March 12, 2014;
posted March 19, 2014 (Doc. ID 204932); published April 11, 2014

We interpret cooperative scattering by a collection of cold atoms as a multiple-scattering process. Starting from microscopic equations describing the response of N atoms to a probe light beam, we represent the total scattered field as an infinite series of multiple-scattering events. As an application of the method, we obtain analytical expressions of the coherent intensity in the double-scattering approximation for Gaussian density profiles. In particular, we quantify the contributions of coherent backward and forward scattering. © 2014 Optical Society of America

OCIS codes: (290.4210) Multiple scattering; (020.1335) Atom optics; (020.1670) Coherent optical effects.
http://dx.doi.org/10.1364/JOSAA.31.001031

1. INTRODUCTION

Multiple scattering of light in disordered media has been investigated for a long time using different approaches [1–3]. Some of them use coupled dipole methods to describe light scattering by dielectric particles [4], while other approaches interpret multiple scattering as a random walk of particle-like photons where interference is neglected. This random walk is described by a radiative transfer equation [5–7], which has been used for decades in astrophysics, where the diffusive behavior is considered as a good description of the light propagation. However, this approach must be corrected when the scattered light wave emerges from the medium in the backward direction. In this case, constructive interferences arises and must be taken into account in order to explain the enhancement of the backscattered intensity with respect to the classical prediction [8–11]. This coherent backscattering (CBS) has been observed for light waves in a variety of media, such as powder suspensions, biological tissues, or Saturn's rings, as well as for laser-cooled atomic gases [12–14]. The latter systems provide an opportunity to observe cooperative effects in the light scattering due to the absence of Doppler broadening.

Recently, a microscopic model of cooperative scattering by cold atoms was proposed [15–19], which accounts for the interference effects. Signatures of cooperativity have been observed in the reduction of the radiation pressure force exerted on the center of mass of the atomic cloud [20,21]. The microscopic model provides an exact description of the scattering of a probe light beam by N atoms, i.e., taking into account interferences. It assumes the incident light beam to be weak enough to neglect nonlinear effects, but naturally embeds the multiple-scattering process of the incoming photons bouncing among the atoms, since the single-atom response is proportional to the sum of the incident field and the field scattered by the other atoms.

The aim of this paper is to characterize the multiple-scattering nature of cooperative scattering, describing it not from the point of view of the atoms, but of the scattered field. Under this view, cooperative scattering appears as a sequence of multiple-scattering events in which the emitted field is expressed as the sum of successively scattered fields. This approach is of particular importance for two reasons. First, scattering in optically dilute systems is very well described by a few scattering events. The number of these events necessary to reconstruct the solution is directly connected to the convergence of the multiple-scattering series. Second, it happens that the multiple-scattering expansion diverges in the optically dense regime. This suggests that the interpretation of multiple scattering as photons wandering from one atom to another one starts to be incomplete. In such a regime, we can only talk about global scattering by the entire cloud, and we lose track of the light propagating in the cloud at different orders of scattering. As a consequence, the scattered field seen by each atom cannot be obtained as the coherent sum over all the light trajectories, but it must result from a global approach, determining either the single-atom response to the total scattered field [22] or the eigenmodes of the system [23].

Let us outline that we treat the light scattering *ab initio*, i.e., considering point-like atoms in the vacuum. This is different from the common approach resorting to an effective Green's function, where the average atomic medium is described by a refractive index, which implies the introduction of a mean free path [5,11,24]. On the contrary, in our model the refractive

index emerges *a posteriori* as a result of the multiple light scattering process [25].

The paper is organized as follows. In Section 2 we review the cooperative scattering model using the more general vectorial model, and show how the atomic response builds up as a reaction to both the incident and scattered fields. The multiple-scattering approach is presented in Section 3. In Section 4 we discuss CBS in the double-scattering approximation, deriving analytical expressions for a Gaussian sphere. We also demonstrate how coherent multiple-scattering theory allows us to obtain corrections to the single-scattering forward emission.

2. MICROSCOPIC APPROACH TO THE COOPERATIVE SCATTERING

The cooperative scattering by N atoms with fixed positions $\mathbf{r}_j$ and illuminated by a monochromatic light beam with electric field components $E^{\alpha}_{\text{in}}(\mathbf{r})\exp(-i\omega t)$ is described by the following set of coupled equations [16,17]:

$$\frac{db^{\alpha}_j}{dt} = (i\Delta - \gamma/2)b^{\alpha}_j - i(d/\hbar)E^{\alpha}_{\text{in}}(\mathbf{r}_j) - (\gamma/2)\sum_{\alpha'}\sum_{m\neq j} G_{\alpha,\alpha'}(\mathbf{r}_j - \mathbf{r}_m)b^{\alpha'}_m, \tag{1}$$

where d is the electric dipole matrix element, $\Delta = \omega - \omega_a$ is the detuning of the incident light frequency $\omega = ck$ from the atomic resonance frequency ω_a, and $\gamma = d^2k^3/3\pi\epsilon_0\hbar$ is the spontaneous decay rate. In the right-hand side of Eq. (1), the first term describes the single-atom dynamics, the second term corresponds to the external field, and the last term describes the radiation of all other atoms on the jth atom. Equation (1) is derived from a quantum approach modeling the scattering of a single photon as being scattered in a mode tailored by the spatial atomic distribution [15,26,27], but also from a classical approach in which the atoms are considered as oscillating dipoles induced by a classical laser field described by the Maxwell equations [16]. The jth atom experiences electric dipole transitions between the single ground state $|g_j\rangle$ and the degenerate triplet excited state $|e^{\alpha}_j\rangle$, where $\alpha = x, y, z$ and b^{α}_j are the probability amplitudes of the single-excitation atomic state $|\Psi\rangle_{\text{e}} = \exp(-i\Delta t)\sum_j\sum_{\alpha} b^{\alpha}_j|g_1,\ldots,e^{\alpha}_j,\ldots,g_N\rangle$. $G_{\alpha,\alpha'}$ are the components of the symmetric tensor:

$$G_{\alpha,\alpha'}(\mathbf{r}) = \frac{3}{2}\frac{e^{ikr}}{ikr}\{[\delta_{\alpha,\alpha'} - \hat{n}_{\alpha}\hat{n}_{\alpha'}] + [\delta_{\alpha,\alpha'} - 3\hat{n}_{\alpha}\hat{n}_{\alpha'}][i/(kr) - 1/(kr)^2]\} \tag{2}$$

with $r = |\mathbf{r}|$ and $\hat{n}_{\alpha}$ being the components of the unit vector $\hat{\mathbf{n}} = \mathbf{r}/r$. The vectorial Green's function (2) can be obtained from the scalar Green's function $G(r) = \exp(ikr)/(ikr)$:

$$G_{\alpha,\alpha'}(\mathbf{r}) = \frac{3}{2}\left[\delta_{\alpha,\alpha'} + \frac{1}{k^2}\frac{\partial^2}{\partial\alpha\partial\alpha'}\right]G(r). \tag{3}$$

The steady-state problem of Eq. (1) boils down to a linear one for the complex vectors $\mathbf{b}_j$ with spatial components b^{α}_j :

$$\mathbf{b}_j = \frac{1}{\Delta + i\gamma/2}\left[\frac{d}{\hbar}\mathbf{E}_{\text{in}}(\mathbf{r}_j) - i\frac{\gamma}{2}\sum_{m\neq j}\mathbf{G}(\mathbf{r}_j - \mathbf{r}_m)\cdot\mathbf{b}_m\right]. \tag{4}$$

Giving the atomic positions $\mathbf{r}_j$ and incident field $\mathbf{E}_{\text{in}}(\mathbf{r}_j)$, it can be solved numerically by inverting a $3N\times 3N$ symmetric matrix.

The scattered field at a position $\mathbf{r}$ is derived from $\mathbf{b}_j$ using the microscopic Maxwell equations for sources of polarization $\mathbf{P}(\mathbf{r}) = -d\sum_j\mathbf{b}_j\delta(\mathbf{r} - \mathbf{r}_j)$. The result, as demonstrated in Appendix A, reads

$$\mathbf{E}_{\text{sca}}(\mathbf{r}) = -i\frac{dk^3}{6\pi\epsilon_0}\sum_{m=1}^{N}\mathbf{G}(\mathbf{r} - \mathbf{r}_m)\cdot\mathbf{b}_m. \tag{5}$$

The scattered field $\mathbf{E}_{\text{sca}}(\mathbf{r}_j)$ at the atomic position $\mathbf{r}_j$ has a divergent contribution in the term $m = j$ of the sum in Eq. (5). This is a well-known problem of the self-field, i.e., the field generated by the atom acting on the atom itself. Usually, in multiple-scattering theories this problem is circumvented by introducing a cut-off length of the order of the size of the real physical scatterer [24]. However, in the present approach the self-field does not play any role. In fact, calling $\mathbf{E}_{\text{self}}(\mathbf{r}_j)$ the self-field of the atom j, Eq. (5) turns into

$$\mathbf{E}_{\text{sca}}(\mathbf{r}_j) = \mathbf{E}_{\text{self}}(\mathbf{r}_j) - i\frac{dk^3}{6\pi\epsilon_0}\sum_{m\neq j}\mathbf{G}(\mathbf{r}_j - \mathbf{r}_m)\cdot\mathbf{b}_m. \tag{6}$$

Combining Eqs. (4) and (6), one can obtain

$$\mathbf{b}_j = \frac{d}{\hbar(\Delta + i\gamma/2)}[\mathbf{E}_{\text{in}}(\mathbf{r}_j) + \bar{\mathbf{E}}(\mathbf{r}_j)], \tag{7}$$

where $\bar{\mathbf{E}}(\mathbf{r}_j) = \mathbf{E}_{\text{sca}}(\mathbf{r}_j) - \mathbf{E}_{\text{self}}(\mathbf{r}_j)$ is the electric field acting on the jth atom without the self-field contribution. $\bar{\mathbf{E}}(\mathbf{r}_j)$ is introduced to describe the field at the atomic positions and avoid the divergence problem present in Eq. (5). The electric dipole moment of each atom $\mathbf{p}_j = -d\mathbf{b}_j$ is directly proportional to the sum of the incident field and the one scattered by all other atoms, as assumed in the cooperative scattering description (4).

3. MULTIPLE-SCATTERING SERIES

In the microscopic approach of cooperative scattering presented in Section 2, the radiation field is determined from the knowledge of the individual atomic responses $\mathbf{b}_j$, which are themselves derived from the linear problem Eq. (4). On the contrary, the multiple-scattering approach is based on a recursive set of equations for the sole radiation field. It is obtained by inserting Eq. (7) back into Eq. (6), leading to an implicit equation for the scattered field $\bar{\mathbf{E}}(\mathbf{r}_j)$ acting on the jth atom:

$$\bar{\mathbf{E}}(\mathbf{r}_j) = \kappa(\delta)\sum_{m\neq j}\mathbf{G}(\mathbf{r}_j - \mathbf{r}_m)\cdot[\mathbf{E}_{\text{in}}(\mathbf{r}_m) + \bar{\mathbf{E}}(\mathbf{r}_m)], \tag{8}$$

where $\kappa(\delta) = 1/(2i\delta - 1)$ and $\delta = \Delta/\gamma$. Introducing the total field $\bar{\mathbf{E}}_{\text{tot}}(\mathbf{r}_j) = \mathbf{E}_{\text{in}}(\mathbf{r}_j) + \bar{\mathbf{E}}(\mathbf{r}_j)$, the above equation can also be written in a matrix form

$$\bar{\mathbf{E}}_{\text{tot}} = (\mathbf{I} - \mathcal{G})^{-1}\mathbf{E}_{\text{in}}, \tag{9}$$

where $\bar{\mathbf{E}}_{\text{tot}}$ and $\mathbf{E}_{\text{in}}$ are vectors containing the $3N$ components of the effective electric field acting on the jth atom (without the self-field contribution) and the incident field, respectively;

I is the $3N \times 3N$ unit matrix, and $\mathcal{G} = \kappa(\delta)\mathbf{G}$ is a $3N \times 3N$ matrix containing the Green's function $\mathbf{G}_{jm} = \mathbf{G}(\mathbf{r}_j - \mathbf{r}_m)$ whose components are given by Eq. (2).

The multiple-scattering approach consists in solving Eq. (8) by iteration. Introducing the scattered field $\bar{\mathbf{E}}^{(n)}$ after n scattering events, the following recurrence relation is obtained from Eq. (9):

$$\bar{\mathbf{E}}^{(n)}(\mathbf{r}_j) = \kappa(\delta)\sum_{m\neq j}\mathbf{G}(\mathbf{r}_j - \mathbf{r}_m)\cdot\bar{\mathbf{E}}^{(n-1)}(\mathbf{r}_m), \tag{10}$$

where $n = 1, 2\ldots$ and the incident field $\bar{\mathbf{E}}^{(0)}(\mathbf{r}_j) = \mathbf{E}_{\text{in}}(\mathbf{r}_j)$ plays the role of the seed. The total scattered field (8) corresponds to the infinite sum of all scattered fields,

$$\bar{\mathbf{E}}(\mathbf{r}_j) = \sum_{n=1}^{\infty}\bar{\mathbf{E}}^{(n)}(\mathbf{r}_j), \tag{11}$$

provided the series is converging. The effective field felt by the scatterer at $\mathbf{r}_j$ consists of the incident wave $\mathbf{E}_{\text{in}}(\mathbf{r}_j)$ and the wave scattered from the other atoms in the cloud (except the self-field of the atom at $\mathbf{r}_j$) given by Eq. (11) and resulting from an increasing number of scattering events of the incident field. Equation (9) can be extended as a series:

$$\bar{\mathbf{E}}_{\text{tot}}(\mathbf{r}_j) = \mathbf{E}_{\text{in}}(\mathbf{r}_j) + \kappa(\delta)\sum_{m\neq j}\mathbf{G}(\mathbf{r}_j - \mathbf{r}_m)\mathbf{E}_{\text{in}}(\mathbf{r}_m) + \kappa^2(\delta)\sum_{m\neq j}\mathbf{G}(\mathbf{r}_j - \mathbf{r}_m)\sum_{l\neq m}\mathbf{G}(\mathbf{r}_m - \mathbf{r}_l)\mathbf{E}_{\text{in}}(\mathbf{r}_l) + \ldots \tag{12}$$

The infinite series (11) converges only if all eigenvalues of $\mathcal{G}$ have their modulus less than unity [28]. When this condition is satisfied, the multiple-scattering expansion can be used to calculate the radiated field.

Note that convergence of the series (11) or of the sum (12) is not tied to the existence of a solution for the field. Indeed Eq. (8) always admits a solution, whereas the linear operator $\mathcal{G}$ of the recurrence Eq. (10) may admit eigenvalues of modulus larger than unity, in which case Eq. (11) does not converge. In that case each scattering order radiates more light than the previous one, and the multiple-scattering expansion diverges. In order to illustrate this point, the electric field profile inside a Gaussian cloud $\mathbf{E}^{(n)}(\mathbf{r}) = \kappa(\delta)\sum_j \mathbf{G}(\mathbf{r} - \mathbf{r}_j)\bar{\mathbf{E}}^{(n-1)}(\mathbf{r}_j)$ and the far-field radiated power $P^{(n)} = (\varepsilon_0 c/2)\int |\mathbf{E}^{(n)}|^2 \mathrm{d}S$ are plotted for different orders n in Figs. 1 and 2, respectively. Both quantities have been obtained for two different optical thicknesses $b(\delta) = b_0/(1 + 4\delta^2)$, where $b_0 = 3N/(k\sigma_R)^2$ is the on-resonant optical thickness for a Gaussian cloud with rms size σ_R. The two simulations have been realized for $N = 500$ atoms with $b_0 = 5$, $\sigma_R = 17.32/k$ and for two different detunings, $\delta = 4.5$ and $\delta = 0$, corresponding to $b(\delta) = 0.061$ and $b(\delta) = 5$, respectively. For the case of small optical thickness ($b(\delta) = 0.061$), the field decreases as the scattering order n increases, and the series (11) converges. For the case of larger optical thickness ($b(\delta) = 5$), the presence of eigenvalues of modulus larger than unity makes the multiple-scattering series diverge. Hence, in the presence of above-unity eigenvalues of $\mathcal{G}$, the multiple-scattering description loses its validity: for sufficiently dense media, due to the long-range interaction of the Green's function, the build-up of the scattered radiation field cannot be seen as the sum of interactions involving an increasing number of atoms, and the local iteration of the scattering event described by Eq. (10) is no longer possible. Instead, the total scattered field is a result of a global interaction with the entire sample. Let us remark that the criterion of all eigenvalues having modulus below unity for the convergence of the series is in agreement with the results of Ref. [29]. A detailed study of the typical spectrum of the linear operator in Eq. (10) has been proposed in [30], yet it is important to mention that the spectrum exhibits strong fluctuations from one realization to another. Since the multiple-scattering process corresponds to a geometric series, the radiated power grows or decreases as a power law of the largest eigenvalue of the linear operator in Eq. (10) for large n.

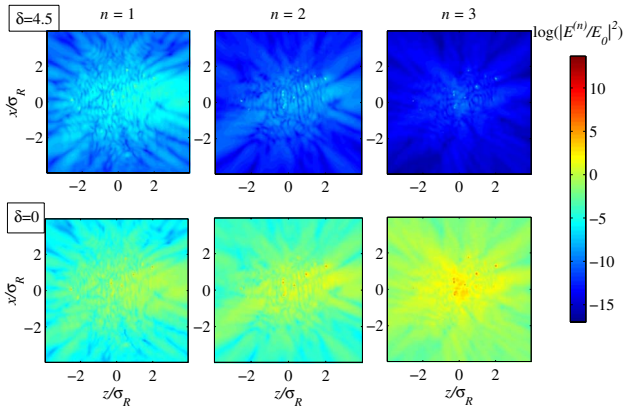

Fig. 1. Profile of the radiation field inside a Gaussian cloud, $\mathbf{E}^{(n)}(\mathbf{r}) = \kappa(\delta)\sum_j \mathbf{G}(\mathbf{r} - \mathbf{r}_j)\bar{\mathbf{E}}^{(n-1)}(\mathbf{r}_j)$, in the $y = 0$ plane for different orders n (from left to right) and two different optical thicknesses (top and bottom). For small optical thickness ($b(\delta) = 0.061$, top line), the field decreases as the scattering order n increases, and the series (10) converges. For larger optical thickness ($b(\delta) = 5$, bottom line), the presence of eigenvalues of modulus larger than unity makes the multiple-scattering series diverge. In both cases, the presence of local fields much stronger than the incident one is due to the divergent field radiated in the vicinity of the atoms, which can be arbitrary close to the $y = 0$ plane. Simulations realized for a Gaussian cloud of $N = 500$ atoms with an on-resonant optical thickness $b_0 = 5$ and standard deviation $\sigma_R = 17.32/k$, where $b_0 = 3N/(k\sigma_R)^2$; top pictures correspond to $\delta = 4.5$ and $b(\delta) = 0.061$, bottom pictures to the resonant case $\delta = 0$ and $b(\delta) = 5$.

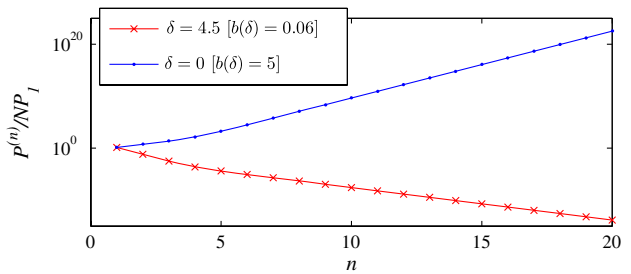

Fig. 2. Far-field power $P^{(n)} = (\varepsilon_0 c/2)\int |\mathbf{E}^{(n)}|^2 \mathrm{d}S$ radiated by the atomic cloud (measured on a spherical surface of radius $r \gg 1/k$) versus the scattering order n for the same parameters as in Fig. 1. For small optical thickness ($b(\delta) = 0.061$, red crosses), the scattered power decreases as the scattering order n increases, whereas for larger optical thickness ($b(\delta) = 5$, blue dots), the power diverges. $P^{(n)}$ is in units of the independent-atom power NP_1, where $P_1 = (4\pi I_0/k^2)/(1 + 4\delta^2)$ and I_0 is the incident intensity.

Once obtained from Eq. (11) $\bar{\mathbf{E}}(\mathbf{r}_j)$, using Eqs. (5) and (7) the scattered field in position $\mathbf{r} \neq \mathbf{r}_j$ is fully determined as

$$\mathbf{E}_{\mathrm{sca}}(\mathbf{r}) = \kappa(\delta) \sum_{j=1}^{N} \mathbf{G}(\mathbf{r} - \mathbf{r}_j) \cdot [\mathbf{E}_{\mathrm{in}}(\mathbf{r}_j) + \bar{\mathbf{E}}(\mathbf{r}_j)]. \tag{13}$$

The multiple-scattering nature of the field detected at $\mathbf{r}$ is evident from Eq. (13): the first term in the sum represents all the single scattering, and the second term collects all the multiple scattering. The $\bar{\mathbf{E}}(\mathbf{r}_j)$ term, which contains all scattering orders starting from the first [see Eq. (11)], yields the double and higher scattering orders in Eq. (13) after applying G.

We point out that the solution for the scattered field [given by the infinite series of Eqs. (11) and (13)] is fully equivalent to solving Eq. (4) for $\mathbf{b}_j$ and then calculating the field using Eq. (5). Equation (4) can be solved exactly by numerical inversion of this linear problem. The only constraint we deal with is the limited number N of scatterers that can be handled by the computer capacities. From the perspective of computing the scattered field, the microscopic approach has a clear advantage over the multiple-scattering one, which requires the evaluation of an infinite sum. The numerical solution of the microscopic approach provides a solution valid for arbitrary distributions of scatterers in the vacuum using only finite matrices. Finally, it treats light as a complex field, not only as an intensity, so that it naturally embeds the coherence of the multiple-scattering process.

In the far-field limit, the scattered field can be derived using the asymptotic form of the vectorial Green's function for $r \gg r_j$:

$$G_{\alpha,\alpha'}(\mathbf{r} - \mathbf{r}_j) \approx \frac{3}{2} \frac{e^{ikr}}{ikr} [\delta_{\alpha,\alpha'} - \hat{n}_\alpha \hat{n}_{\alpha'}] e^{-i\mathbf{k}\cdot\mathbf{r}_j}, \tag{14}$$

where $\mathbf{k} = k\hat{\mathbf{n}}$. For an incident plane wave with $\mathbf{E}_{\mathrm{in}}(\mathbf{r}) = \hat{\mathbf{e}}_0 E_0 \exp(i\mathbf{k}_0 \cdot \mathbf{r})$, where $\hat{\mathbf{e}}_0$ is the unit polarization vector, the scattered far field derived from Eq. (13) is

$$\mathbf{E}_{\mathrm{sca}}^{\mathrm{far}}(\mathbf{r}) = \mathbf{E}_1^{\mathrm{far}}(\mathbf{r}) + \mathbf{E}_{\mathrm{ms}}^{\mathrm{far}}(\mathbf{r}), \tag{15}$$

where

$$\mathbf{E}_1^{\mathrm{far}}(\mathbf{r}) = \kappa(\delta) E_0 \frac{e^{ikr}}{ikr} [\hat{\mathbf{n}} \times (\hat{\mathbf{n}} \times \hat{\mathbf{e}}_0)] N S_N(\mathbf{k} - \mathbf{k}_0) \tag{16}$$

corresponds to the single-scattering order and $S_N(\mathbf{k} - \mathbf{k}_0) = (1/N)\sum_j \exp[-i(\mathbf{k} - \mathbf{k}_0) \cdot \mathbf{r}_j]$ is the structure factor. Equation (16) is the well-known expression for the Rayleigh scattering by particles with size much smaller than the optical wavelength when each atom is excited by the incident field only. Then the scattered field results from a coherent superposition of the field amplitudes generated by each atom and is proportional to the structure factor. The multiple-scattering contribution to the far field of Eq. (15) is, using Eq. (11),

$$\mathbf{E}_{\mathrm{ms}}^{\mathrm{far}}(\mathbf{r}) = \kappa(\delta) \frac{e^{ikr}}{ikr} N \hat{\mathbf{n}} \times [\hat{\mathbf{n}} \times \mathbf{F}(\mathbf{k})], \tag{17}$$

where

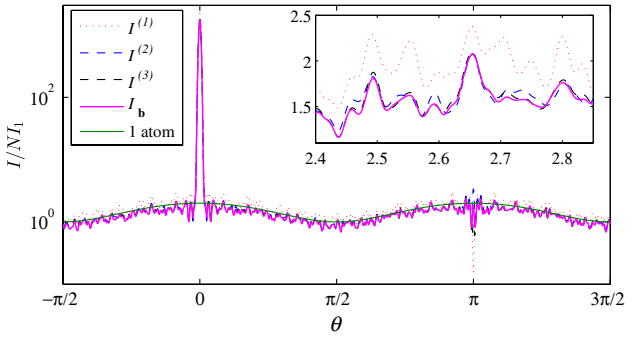

Fig. 3. Intensity diagram, $I^{(n)} = (\varepsilon_0 c/2)|\sum_{j=1}^{n} \mathbf{E}^{(j)}|^2$, versus the polar angle θ, for $n = 1, 2, 3$, derived from Eq. (13). The intensity scattered by the dipoles, $I_{\mathbf{b}} = (\varepsilon_0 c/2)|\mathbf{E}_{\mathbf{b}}|^2$, is derived from Eq. (4) and contains all the scattering orders. The modulation of the background is due to the vectorial nature of the light (linearly polarized light): the single-atom intensity $I_1(1 + \cos^2\theta)$ is plotted as a plain green line, where $I_1 = I_0/[k^2 r^2 (1 + 4\delta^2)]$. The inset shows a zoom of the radiation (linear scale). Simulations have been realized for a Gaussian cloud of $N = 1000$ atoms with on-resonance optical thickness $b_0 = 1$, detuning $\delta = 0$, and rms size $\sigma_R \approx 54.8/k$ given by $b_0 = 3N/(k\sigma_R)^2$. The intensity is averaged over the azimuthal angle ϕ and is in units of NI_1.

$$\mathbf{F}(\mathbf{k}) = \frac{1}{N} \sum_{j=1}^{N} \bar{\mathbf{E}}(\mathbf{r}_j) e^{-i\mathbf{k}\cdot\mathbf{r}_j}. \tag{18}$$

We stress that our approach is valid beyond the single-scattering limit. The single-scattering approximation holds when the optical thickness $b(\delta) = b_0/(1 + 4\delta^2)$ is much smaller than unity. In contrast, our multiple-scattering approach is valid for finite values of $b(\delta) < 1$: the convergence of the series of Eq. (11) guarantees the validity of our multiple-scattering expansion [31,32].

Finally, we emphasize that if the infinite sum in Eq. (11) converges, it gives the *exact* solution for the collective scattering problem given by Eqs. (4) and (5). To illustrate this point, we compare the intensity radiated up to the nth order $I^{(n)} = (\varepsilon_0 c/2)|\sum_{j=1}^{n} \mathbf{E}^{(j)}|^2$ for $n = 1, 2, 3$, as well as the intensity $I_{\mathbf{b}}$ provided by the dipole amplitudes $\mathbf{b}_m$ derived from Eq. (4) and containing all the scattering orders. In particular, $I^{(1)}$ describes the single scattering only, $I^{(2)}$ the sum of single and double scattering, etc. For an optical thickness $b(\delta)$ equal to unity ($b_0 = 1$, $\delta = 0$), the convergence is relatively slow, but clearly visible in Fig. 3. For optical thickness much smaller than unity, the convergence is very fast and the single-scattering physics contained in $\mathbf{E}^{(1)}$ describes already very well the total scattered field (not shown here).

We note in Fig. 3 that the coupled dipole equation predicts a background radiation lower than N times that of a single atom. This suggests a reduction of the background radiation, in favor of the coherent forward radiation, under the effects of cooperativity. This effect will be the subject of a future dedicated study.

4. COHERENT BACKWARD AND FORWARD SCATTERING

As an application of the multiple-scattering approach, we investigate CBS and coherent forward scattering (CFS) from a collection of N atoms. For the sake of simplicity, we assume that the radiation waves are scalar, neglecting polarization and near-field effects. In the scalar radiation theory, the three

components b_j^α in Eq. (1) are replaced by a single value β_j, the vectorial kernel $G_{\alpha,\alpha'}(\mathbf{r})$ is substituted by the scalar Green's function $G(r) = \exp(ikr)/(ikr)$, and the decay constant γ is replaced by $\Gamma = (3/2)\gamma$ [18,33,34]. Then, the scalar equivalent of Eq. (13) is

$$E_{\mathrm{sca}}(\mathbf{r}) = \kappa(\delta)\sum_{j=1}^{N} G(|\mathbf{r}-\mathbf{r}_j|)[E_{\mathrm{in}}(\mathbf{r}_j) + \bar{E}(\mathbf{r}_j)]. \tag{19}$$

We approximate the multiple-scattering field $\bar{E}(\mathbf{r}_j)$ by its first contribution:

$$\bar{E}(\mathbf{r}_j) \approx \kappa(\delta)\sum_{m\neq j} G(|\mathbf{r}_j-\mathbf{r}_m|)E_{\mathrm{in}}(\mathbf{r}_m), \tag{20}$$

which is equivalent to considering single- and double-scattering events only:

$$E_{\mathrm{tot}}(\mathbf{r}) = E_{\mathrm{in}}(\mathbf{r}) + \kappa(\delta)\sum_{j=1}^{N} G(|\mathbf{r}-\mathbf{r}_j|)E_{\mathrm{in}}(\mathbf{r}_j) + \kappa^2(\delta)\sum_{m=1}^{N}\sum_{j\neq m} G(|\mathbf{r}-\mathbf{r}_m|)G(|\mathbf{r}_m-\mathbf{r}_j|)E_{\mathrm{in}}(\mathbf{r}_j). \tag{21}$$

The second term in Eq. (21) describes the single scattering of the incident wave by each atom in position $\mathbf{r}_j$, followed by its propagation toward $\mathbf{r}$. The third term corresponds to the double-scattering contribution; i.e., the photons are first scattered by the atoms in $\mathbf{r}_j$, then propagate to $\mathbf{r}_m$, where they are scattered again and reach position $\mathbf{r}$. As it can be observed in Fig. 4, the double scattering is the first of the multiple-scattering processes that contributes to CBS. It results from the interference between the wave that is first scattered in $\mathbf{r}_j$ and then in $\mathbf{r}_m$, and the reciprocal path, when the wave is first scattered in $\mathbf{r}_m$ and then in $\mathbf{r}_j$. This effect can be captured by calculating the scattered field in the far-field limit, approximating the Green's function as $G(|\mathbf{r}-\mathbf{r}_j|) \approx \exp(ikr - i\mathbf{k}\cdot\mathbf{r}_j)/(ikr)$:

$$E_{\mathrm{sca}}(\mathbf{r}) = \kappa(\delta)\frac{e^{ikr}}{ikr}E_0\sum_{j=1}^{N} e^{i(\mathbf{k}_0-\mathbf{k})\cdot\mathbf{r}_j} + \kappa^2(\delta)\frac{e^{ikr}}{ikr}E_0\sum_{m=1}^{N}\sum_{j\neq m} G(|\mathbf{r}_m-\mathbf{r}_j|)e^{i(\mathbf{k}_0\cdot\mathbf{r}_j-\mathbf{k}\cdot\mathbf{r}_m)}, \tag{22}$$

where we assume that the incident field is a plane wave $E_{\mathrm{in}}(\mathbf{r}) = E_0\exp(i\mathbf{k}_0\cdot\mathbf{r})$. Introducing the factor

$$T_N(\mathbf{k},\mathbf{k}_0) = \frac{1}{N}\sum_{m}\sum_{j\neq m} G(|\mathbf{r}_j-\mathbf{r}_m|)e^{i(\mathbf{k}_0\cdot\mathbf{r}_j-\mathbf{k}\cdot\mathbf{r}_m)}, \tag{23}$$

the scattered intensity up to the second scattering order can be written as

$$I_{\mathrm{sca}}(\mathbf{r}) = I_1 N^2|S_N(\mathbf{k}-\mathbf{k}_0) + \kappa(\delta)T_N(\mathbf{k},\mathbf{k}_0)|^2, \tag{24}$$

where $I_1 = I_0/[k^2r^2(1+4\delta^2)]$ is the single-atom scattered intensity and I_0 is the intensity of the incident wave. Upon configuration averaging, the structure factor gives an incoherent contribution, $|S_N(\mathbf{k}-\mathbf{k}_0)|^2 = 1/N$, while the coherent contribution in the forward direction for large N can be written as a continuous integral:

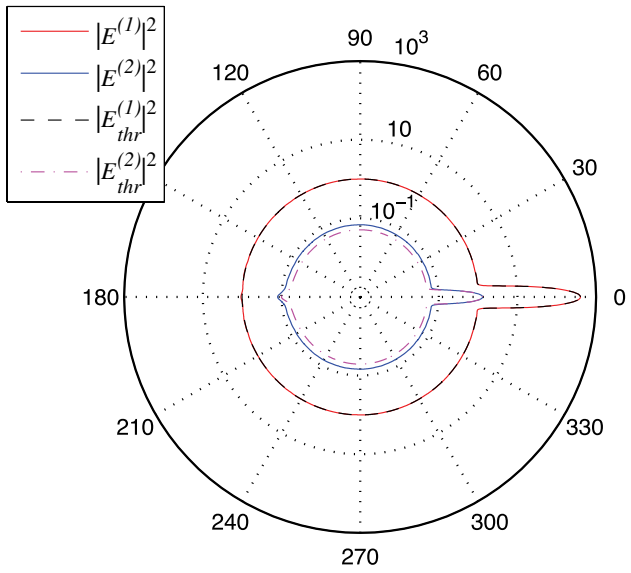

Fig. 4. Radiation profile $|E^{(n)}(\theta)|^2$ in the far-field limit for scattering orders $n = 1, 2$. The single-scattering order $E^{(1)}$ exhibits only a forward contribution (peaks pointing to the right) and a homogeneous background. The double-scattering contribution $E^{(2)}$ shows both forward and backward (CBS) patterns (peaks pointing to the left) in addition to the background. The theoretical curves (thr) are derived from Eqs. (30), (31), and (32). Simulations are realized for a Gaussian spherical cloud consisting of $N = 400$ atoms with resonant optical thickness $b_0 = 2N/(k\sigma_R)^2 = 1$, standard deviation $\sigma_R \approx 28.3/k$, and detuning $\delta = 1$, and averaged over 1000 realizations. The incoming field is unity $E_0 = 1$, and the radius of observation is $3\cdot 10^4/k$. Scale is logarithmic.

$$S_\infty = \frac{1}{N}\int d\mathbf{r}\rho(\mathbf{r})\exp[i(\mathbf{k}-\mathbf{k}_0)\cdot\mathbf{r}], \tag{25}$$

where $\rho(\mathbf{r})$ is the atomic density. $|T_N|^2$ yields an incoherent contribution plus two coherent contributions, which, however, have different origins. Taking the square modulus of Eq. (23) and considering only equal pairs of atoms (j,m) in T_N and T_N^*, we obtain

$$|T_N(\mathbf{k},\mathbf{k}_0)|^2_{\mathrm{pair}} \approx \frac{1}{N^2}\sum_{m}\sum_{j\neq m}\frac{1+\cos[(\mathbf{k}+\mathbf{k}_0)\cdot(\mathbf{r}_j-\mathbf{r}_m)]}{k^2|\mathbf{r}_j-\mathbf{r}_m|^2}. \tag{26}$$

The first incoherent term emerges when the same pair of atoms is considered twice [$1/k^2|\mathbf{r}_j-\mathbf{r}_m|^2$ term in Eq. (26)], whereas the second term results from the pair (j,m) crossed with its reciprocal path (m,j) (cosine term). The latter is known as the CBS term [8], since it also yields a backward coherent radiation. In the diagrammatic approach, the first term in Eq. (26) corresponds to the first 'ladder' term, and the second one to the 'most-crossed term' [24]. Besides these pair terms, T_N also gives a coherent contribution to the forward intensity due to the processes involving more than two atoms. This contribution in the continuous density limit can be written as

$$T_\infty(\mathbf{k},\mathbf{k}_0)=\frac{1}{N}\int d\mathbf{r}_1\rho(\mathbf{r}_1)\int d\mathbf{r}_2\rho(\mathbf{r}_2)\frac{\exp(ik|\mathbf{r}_1-\mathbf{r}_2|)}{ik|\mathbf{r}_1-\mathbf{r}_2|}\times e^{i(\mathbf{k}_0\cdot\mathbf{r}_1-\mathbf{k}\cdot\mathbf{r}_2)}. \quad (27)$$

Collecting the different contributions, the scattered intensity up to the double-scattering order reads

$$I_{\mathrm{sca}}=I_1N\left\{1+\frac{N}{1+4\delta^2}|T_N|^2_{\mathrm{pair}}+N|F|^2\right\}, \quad (28)$$

where $F=S_\infty+\kappa(\delta)T_\infty$. The first term is the isotropic incoherent contribution NI_1 of N independent atoms. The second term enhances the previous incoherent term and also provides the CBS cone [second term in Eq. (26)]. Finally, the third term in Eq. (28) contributes to the coherent forward emission as the sum of the single- and double-scattering contributions.

The CBS cone reveals itself upon averaging over the pair double-scattering term (26). We first average over the direction of the vector $\mathbf{r}_j-\mathbf{r}_m$, assuming an atomic distribution with infinite boundaries, as, for instance, the Gaussian one, which is easy to parametrize. Moreover, there is no need to know the details about the density of the cloud, since we deal with angular variables only. We note that although the procedure does not correspond to a rigorous configuration average, it allows for analytical results and compares well with numerical results obtained by configuration averages (see Fig. 4).

This first averaging results in (see Appendix B for details)

$$\langle|T_N|^2_{\mathrm{pair}}\rangle=\frac{1}{N^2}\sum_j\sum_{m\neq j}\frac{1}{k^2r_{jm}^2}\times\left\{1+\frac{\sin[2kr_{jm}\cos(\theta/2)]}{2kr_{jm}\cos(\theta/2)}\right\}. \quad (29)$$

where θ refers to the angle of $\mathbf{k}$ with respect to the direction of $\mathbf{k}_0$. The average over the pair distance $r_{jm}=|\mathbf{r}_j-\mathbf{r}_m|$ is the next step, and the resulting backscattering enhancement depends on the atomic distribution. In the next section, we discuss the CBS for Gaussian spheres.

A. Gaussian Sphere Density Profile

As discussed previously, our multiple-scattering approach is valid for arbitrary geometries, including inhomogeneous media. Let us illustrate this on a Gaussian sphere of standard deviation σ_R, for which the contribution of double scattering to CBS enhancement reads (see Appendix C)

$$\langle|T_N(\theta)|^2_{\mathrm{pair}}\rangle=\frac{1}{2\sigma^2}\left\{1+\frac{\sqrt{\pi}}{2}\frac{\mathrm{erf}[2\sigma\cos(\theta/2)]}{2\sigma\cos(\theta/2)}\right\}=\frac{E(\theta)}{2\sigma^2} \quad (30)$$

with $\sigma=k\sigma_R$. $E(\theta)$ has a maximum enhancement of 2 (see Fig. 6) and an angular FWHM of $\Delta\theta=2\sqrt{3}/\sigma\approx0.55(\lambda/\sigma_R)$.

For a Gaussian sphere, the single-scattering forward contribution gives (see Ref. [17], Eq. (25))

$$S_\infty(\theta)=\exp[-2\sigma^2\sin^2(\theta/2)], \quad (31)$$

while the second-order forward contribution, in the limit of large spheres $\sigma\gg1$, is

$$T_\infty(\theta)\approx\frac{N}{4\sigma^2}\exp[-4\sigma^2\sin^2(\theta/4)]. \quad (32)$$

The exact expression and its derivation are given in Appendix D. The total scattered intensity for a Gaussian sphere, up to the second scattering order [see Eq. (28)], reads

$$I_{\mathrm{sca}}(\mathbf{r})=I_1N\left\{1+\frac{b(\delta)}{4}E(\theta)+N|F(\theta)|^2\right\}, \quad (33)$$

where the forward contribution is given by

$$F(\theta)=e^{-2\sigma^2\sin^2(\theta/2)}-(1+2i\delta)\frac{b(\delta)}{8}e^{-4\sigma^2\sin^2(\theta/4)}, \quad (34)$$

and $b(\delta)=b_0/(1+4\delta^2)$ with $b_0=2N/\sigma^2$ being the resonant optical thickness for scalar light. Equation (34) highlights the fact that the multiple-scattering expansion is performed in orders of $b(\delta)=\sqrt{2\pi}(\sigma_R/\ell)$, i.e., in orders of inverse scattering mean free path $\ell=1/[\rho_0\sigma_{\mathrm{sc}}(\delta)]$, where $\sigma_{\mathrm{sc}}(\delta)=4\pi/[k^2(1+4\delta^2)]$ is the scattering cross section.

The background second-order scattering is observed to interfere destructively with the background first-order scattering in Fig. 5, leading to an overall reduction of the background radiation. This effect is already present in the mathematical expression of the forward contribution given by Eq. (34), which is expected to be the dominant term except for the backward direction.

Coherent Backscattering. Our analysis is in excellent agreement with the experimental results of Bidel and coworkers [13]; see Fig. 6. These authors probed the CBS cone for a large cloud ($\sigma=8098$) of scalar optical thickness $b_0=1.93$ at resonance, and measured an angular width of the cone of 0.50 ± 0.04 mrad. This result is in accord with the theoretical value of 0.46 mrad derived from Eq. (30).

Coherent Forward Scattering. —The single-scattering forward lobe is given by the first term in Eq. (34), and reflects the diffraction from the sample. Surprisingly, we also observe a forward lobe for the double-scattering contribution, given by the second term in Eq. (34). The ratio between the peak intensity of the double scattering compared to that of single scattering is always given by $b_0^2/64(4\delta^2+1)$, and the ratio of

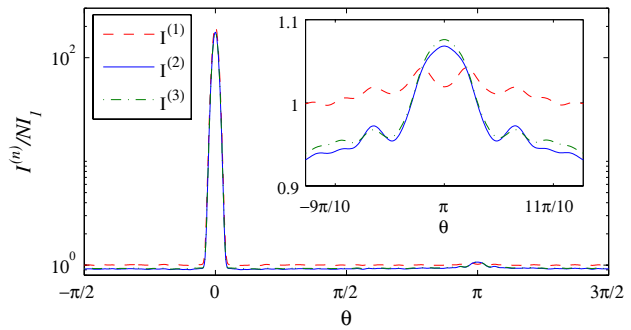

Fig. 5. Far-field scattered intensity versus θ up to the first, second, and third scattering orders, i.e., $I^{(n)}=(\varepsilon_0c/2)|\sum_{j=1}^n E^{(j)}|^2$, in units of NI_1. The inset is a zoom of the backscattering region (linear scale). Simulations realized for a Gaussian spherical cloud of on-resonant optical thickness $b_0=1$, $N=200$ particles, scaled size $\sigma=20$, and laser detuning $\delta=0.5$. The intensity has been averaged over 1000 realizations.

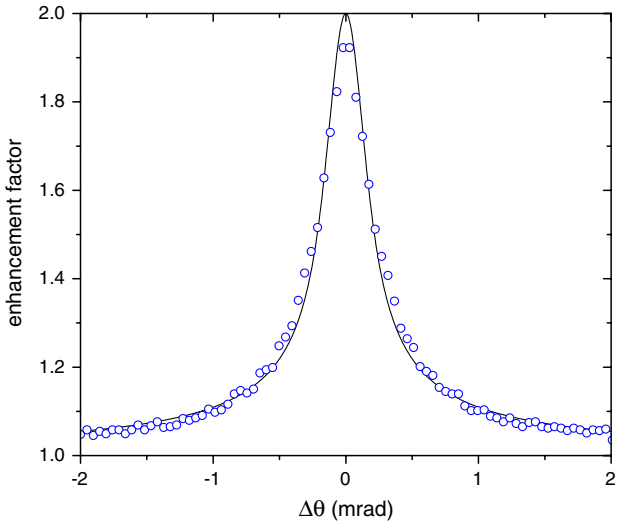

Fig. 6. Experimental and theoretical CBS enhancement $E(\theta)$ for a Gaussian sphere of normalized standard deviation $\sigma = 8098$ and $\delta = 0$. The circles correspond to the experimental values reported in Fig. 2 of Ref. [13], while the plain curve reproduces Eq. (33). It must be noted that the only free parameter is a 3% adjustment of the background.

their power by $b_0^2/32(4\delta^2+1)$ for $\sigma \gg 1$, independently of spatial density.

We, however, note that increasing the system size at constant b_0 and δ will increase the peak amplitude and power for both the first and second scattering orders [last N factor in Eq. (33)], yet their ratio remains constant. This CFS lobe could be compared to that of Refs. [35,36]. In both these works, the forward lobe appears only in the high spatial density limit close to the Anderson localization threshold, whereas in our case, the lobe is also present in the low-density limit.

5. CONCLUSION

We have proposed an iterative multiple-scattering approach, where the radiation field at each scattering order is obtained from the field at the atomic positions calculated at the previous order. Provided all the eigenvalues of the iterative scattering operator have below-unity eigenvalues, it provides a converging solution for the multiple-scattering problem. In the opposite case, the picture of waves being scattered at one atom after the other collapses, and the multiple-scattering series becomes divergent. A limitation of the approach is that the derivation of the n th scattering order involves $n-1$ integrals over the cloud distribution, which practically limits the efficiency of the method to the first scattering orders for nontrivial geometries.

On the other hand, the series permits us to link observable phenomena to particular scattering orders, thus deepening our understanding of their physical origin. As an example, for arbitrary distributions we calculate the double-scattering contributions to backward coherent radiation, the so-called CBS cone.

Finally, the multiple-scattering approach presented in this paper may find applications in other many-body scattering problems. One such example is the elucidation of the relationship between Bragg scattering and the phenomenon of photonic bandgaps, the first one occurring in the single- and the second one in the multiple-scattering regime.

APPENDIX A: DERIVATION OF EQ. (5)

The radiation field can be obtained from Maxwell equations in the presence of a polarization $\mathbf{P}$. The equations for the Fourier component at the frequency $\omega = ck$ are

$$\nabla \times \mathbf{E} = i\omega \mathbf{B}, \tag{A1}$$

$$\nabla \times \mathbf{B} = -i\omega\mu_0(\epsilon_0 \mathbf{E} + \mathbf{P}), \tag{A2}$$

$$\nabla \cdot \mathbf{E} = -(1/\epsilon_0)\nabla \cdot \mathbf{P}. \tag{A3}$$

Taking the curl of Eq. (A1) and using Eq. (A2),

$$\nabla \times \nabla \times \mathbf{E} = (\omega^2/c^2)[\mathbf{E} + (1/\epsilon_0)\mathbf{P}], \tag{A4}$$

where $c = (\varepsilon_0\mu_0)^{-1/2}$ is the vacuum speed of light. Using the identity $\nabla \times \nabla \times \mathbf{E} = \nabla(\nabla \cdot \mathbf{E}) - \nabla^2\mathbf{E}$ and Eq. (A3), we obtain

$$(\nabla^2 + k^2)\mathbf{E} = -\frac{k^2}{\epsilon_0}\left[\mathbf{P} + \frac{1}{k^2}\nabla(\nabla \cdot \mathbf{P})\right]. \tag{A5}$$

The solution of Eq. (A5) is easily obtained using the scalar Green's function $G(r) = \exp(ikr)/(ikr)$ as

$$\mathbf{E}(\mathbf{r}) = i\frac{k^3}{4\pi\epsilon_0}\int d\mathbf{r}' G(|\mathbf{r}-\mathbf{r}'|)\left[\mathbf{P}(\mathbf{r}') + \frac{1}{k^2}\nabla(\nabla \cdot \mathbf{P}(\mathbf{r}'))\right] \tag{A6}$$

or, for each component,

$$E_\alpha(\mathbf{r}) = i\frac{k^3}{4\pi\epsilon_0}\sum_\beta \int d\mathbf{r}' G(|\mathbf{r}-\mathbf{r}'|) \times \left[\delta_{\alpha,\beta} + \frac{1}{k^2}\frac{\partial^2}{\partial x'_\alpha \partial x'_\beta}\right] P_\beta(\mathbf{r}'). \tag{A7}$$

By integrating by parts and using Eq. (3), we obtain

$$E_\alpha(\mathbf{r}) = i\frac{k^3}{6\pi\epsilon_0}\sum_\beta \int d\mathbf{r}' G_{\alpha,\beta}(\mathbf{r}-\mathbf{r}')P_\beta(\mathbf{r}'). \tag{A8}$$

Taking a discrete distribution of electric dipoles, with $\mathbf{P}(\mathbf{r}) = -d\sum_{j=1}^N \mathbf{b}_j \delta(\mathbf{r}-\mathbf{r}_j)$, we obtain

$$\mathbf{E}(\mathbf{r}) = -i\frac{dk^3}{6\pi\epsilon_0}\sum_{m=1}^N \mathbf{G}(\mathbf{r}-\mathbf{r}_m)\cdot\mathbf{b}_m. \tag{A9}$$

APPENDIX B: AVERAGE OVER RANDOM ANGULAR VARIABLES FOR THE CBS CONTRIBUTION

Assuming in the double-scattering contribution of Eq. (26) $\mathbf{k}_0 = k(0,0,1)$, $\mathbf{k} = k(\sin\theta\cos\phi, \sin\theta\sin\phi, \cos\theta)$, and $\mathbf{r}_{jm} = r_{jm}(\sin\theta_{jm}\cos\phi_{jm}, \sin\theta_{jm}\sin\phi_{jm}, \cos\theta_{jm})$, where $\mathbf{r}_{jm} = \mathbf{r}_j - \mathbf{r}_m$, then

$$(\mathbf{k}+\mathbf{k}_0)\cdot\mathbf{r}_{jm} = kr_{jm}[\sin\theta\sin\theta_{jm}\cos(\phi_{jm}-\phi) + (1+\cos\theta)\cos\theta_{jm}]. \tag{B1}$$

By averaging over θ_{jm} and ϕ_{jm}, we obtain

$$\langle |T_N|^2_{\text{pair}} \rangle = \frac{1}{N^2} \sum_{j,m\neq j} \frac{1}{k^2 r_{jm}^2} \times \left\{ 1 + \frac{1}{4\pi} \int_0^{2\pi} \mathrm{d}\phi_{jm} \int_0^{\pi} \mathrm{d}\theta_{jm} \sin\theta_{jm} \times \cos\{kr_{jm}[\sin\theta \sin\theta_{jm} \cos(\phi_{jm} - \phi) + (1 + \cos\theta)\cos\theta_{jm}]\} \right\}. \quad \text{(B2)}$$

Using the expression $\int_0^{2\pi} \mathrm{d}\phi \cos[a + b\cos(\phi - \phi')] = 2\pi \cos(a) J_0(b)$, the integration over ϕ_{jm} gives

$$\langle |T_N|^2_{\text{pair}} \rangle = \frac{1}{N^2} \sum_j \sum_{m\neq j} \frac{1}{kr_{jm}^2} \times \left\{ 1 + \frac{1}{2} \int_0^{\pi} \mathrm{d}\theta_{jm} \sin\theta_{jm} \times \cos[kr_{jm}(1 + \cos\theta)\cos\theta_{jm}] \times J_0[kr_{jm} \sin\theta \sin\theta_{jm}] \right\}. \quad \text{(B3)}$$

Using the expression

$$\int_0^{\pi} \mathrm{d}\theta \sin\theta \cos(a\cos\theta) J_0(b\sin\theta) = 2\frac{\sin\sqrt{a^2 + b^2}}{\sqrt{a^2 + b^2}}, \quad \text{(B4)}$$

we obtain

$$\langle |T_N|^2_{\text{pair}} \rangle = \frac{1}{N^2} \sum_j \sum_{m\neq j} \frac{1}{kr_{jm}^2} \{1 + \text{sinc}[2kr_{jm}\cos(\theta/2)]\}, \quad \text{(B5)}$$

where $\text{sinc}(z) = \sin(z)/z$.

APPENDIX C: DERIVATION OF EQ. (30)

Let us consider the integral

$$I = \int \mathrm{d}\mathbf{r}_1 \rho(\mathbf{r}_1) \int \mathrm{d}\mathbf{r}_2 \rho(\mathbf{r}_2) f(|\mathbf{r}_1 - \mathbf{r}_2|). \quad \text{(C1)}$$

Changing integration variables from $\mathbf{r}_1$ and $\mathbf{r}_2$ to $\mathbf{R} = (\mathbf{r}_1 + \mathbf{r}_2)/2$ and $\mathbf{s} = \mathbf{r}_1 - \mathbf{r}_2$,

$$I = \int \mathrm{d}\mathbf{R} \int \mathrm{d}\mathbf{s} \rho(\mathbf{R} - \mathbf{s}/2)\rho(\mathbf{R} + \mathbf{s}/2) f(|\mathbf{s}|). \quad \text{(C2)}$$

Assuming a Gaussian distribution, $\rho(\mathbf{r}) = \rho_0 \exp(-r^2/2\sigma_R^2)$, since $|\mathbf{R} + \mathbf{s}/2|^2 + |\mathbf{R} - \mathbf{s}/2|^2 = 2R^2 + s^2/2$, in polar coordinates the integral (C1) becomes

$$I = \frac{2N^2}{\pi\sigma_R^6} \int_0^{\infty} \mathrm{d}R R^2 e^{-R^2/\sigma_R^2} \int_0^{\infty} \mathrm{d}s s^2 e^{-s^2/4\sigma_R^2} f(s) = \frac{4N^2}{\sqrt{\pi}} \int_0^{\infty} \mathrm{d}x x^2 e^{-x^2} f(2\sigma_R x). \quad \text{(C3)}$$

Taking

$$f(s) = \frac{1}{k^2 s^2} \left\{ 1 + \frac{\sin[2ks\cos(\theta/2)]}{2sk\cos(\theta/2)} \right\}, \quad \text{(C4)}$$

the integral is

$$I = \frac{N^2}{\sigma^2\sqrt{\pi}} \int_0^{\infty} \mathrm{d}x e^{-x^2} \left[1 + \frac{\sin(ax)}{ax} \right] = \frac{N^2}{2\sigma^2} \left[1 + \frac{\sqrt{\pi}}{a} \text{erf}(a/2) \right], \quad \text{(C5)}$$

where $\sigma = k\sigma_R$ and $a = 4\sigma\cos(\theta/2)$.

APPENDIX D: DERIVATION OF EQ. (32)

Let us consider the coherent contribution $T_\infty(\mathbf{k}, \mathbf{k}_0)$ of Eq. (27) and introduce $\mathbf{R} = (\mathbf{r}_1 + \mathbf{r}_2)/2$ and $\mathbf{s} = \mathbf{r}_1 - \mathbf{r}_2$, so that

$$T_\infty(\mathbf{k}, \mathbf{k}_0) = \frac{1}{ikN} \int \mathrm{d}\mathbf{R} \int \mathrm{d}\mathbf{s} \rho(\mathbf{R} + \mathbf{s}/2)\rho(\mathbf{R} - \mathbf{s}/2) \times s^{-1} e^{i(\mathbf{k}_0 - \mathbf{k})\cdot\mathbf{R} + i(\mathbf{k}_0 + \mathbf{k})\cdot\mathbf{s}/2 + iks}. \quad \text{(D1)}$$

For a Gaussian distribution the double integral factorizes,

$$T_\infty(\mathbf{k}, \mathbf{k}_0) = \frac{\rho_0^2}{ikN} \int \mathrm{d}\mathbf{R} e^{-R^2/\sigma_R^2 + i(\mathbf{k}_0 - \mathbf{k})\cdot\mathbf{R}} \times \int \mathrm{d}s s^{-1} e^{-s^2/4\sigma_R^2 + i(\mathbf{k}_0 + \mathbf{k})\cdot\mathbf{s}/2 + iks}. \quad \text{(D2)}$$

Assuming $\mathbf{k} = (\sin\theta\cos\phi, \sin\theta\sin\phi, \cos\theta)$ and $\mathbf{k}_0 = k(0, 0, 1)$, the first integral yields

$$I_1 = \rho_0 \int \mathrm{d}\mathbf{R} e^{-R^2/\sigma_R^2 + i(\mathbf{k}_0 - \mathbf{k})\cdot\mathbf{R}} = \frac{N}{2\sqrt{2}} e^{-\sigma^2(1 - \cos\theta)/2},$$

where $\sigma = k\sigma_R$. The second integral of Eq. (D2), after integration over the angular variables, yields

$$I_2 = \frac{2N}{i\sqrt{2\pi}\sigma^2\cos(\theta/2)} \int_0^{\infty} \mathrm{d}x e^{-x^2/4 + i\sigma x} \sin[\sigma\cos(\theta/2)x].$$

Using the expression

$$\int_0^{\infty} \mathrm{d}x e^{-x^2/4 + iax} \sin(bx) = \frac{\sqrt{\pi}}{2} \{-e^{4ab}[\text{erfi}(a - b) - i] + \text{erfi}(a + b) - i\} e^{-(a+b)^2} \quad \text{(D3)}$$

we obtain, from the above equations

$$T_\infty(\theta) = \frac{Ne^{-2\sigma^2(1+\cos\theta/2)}}{4i\sigma^2\cos\theta/2} \{\text{erfi}[\sigma(1 + \cos\theta/2)] - e^{4\sigma^2\cos\theta/2}\text{erfi}[\sigma(1 - \cos\theta/2)] + i(e^{4\sigma^2\cos\theta/2} - 1)\}. \quad \text{(D4)}$$

Notice that $T_\infty(\pi) = N\exp(-2\sigma^2)$. For large σ and near the forward direction, we get

$$T_\infty(\theta) \approx \frac{N}{4\sigma^2} e^{-4\sigma^2\sin^2(\theta/4)} \approx \frac{b_0}{8} e^{-4\sigma^2\sin^2(\theta/4)}. \quad \text{(D5)}$$

ACKNOWLEDGMENTS

We acknowledge financial support from the Research Executive Agency (Program COSCALI, grant No. PIRSES-GA-2010-268717), from USP/COFECUB (project Uc Ph 123/11),

and from GDRI "NANOMAGNETISM, SPIN ELECTRONICS, QUANTUM OPTICS AND QUANTUM TECHNOLOGIES." M.T.R. is supported by an Averroès exchange program. R. B. and Ph. W. C. acknowledge support from the Fundação de Amparo à Pesquisa do Estado de São Paulo (FAPESP).

REFERENCES

1. M. C. W. van Rossum and T. M. Nieuwenhuizen, "Multiple scattering of classical waves: microscopy, mesoscopy, and diffusion," Rev. Mod. Phys. **71**, 313–371 (1999).
2. M. I. Mishchenko, L. D. Travis, and A. A. Lacis, *Multiple Scattering of Light by Particles: Radiative Transfer and Coherent Backscattering* (Cambridge University, 2006).
3. E. Akkermans and G. Montambaux, *Mesoscopic Physics of Electrons and Photons*, 1st ed. (Cambridge University, 2007).
4. E. M. Purcell and C. R. Pennypacker, "Scattering and absorption by nonsphereical dielectric grains," Astrophys. J. **186**, 705–714 (1973).
5. A. Ishimaru, *Wave Propagation and Scattering in Random Media and Rough Surfaces*, Vol. **2** (Academic, 1978).
6. A. Ishimaru, "Wave propagation and scattering in random media and rough surfaces," Proc. IEEE **79**, 1359–1366 (1991).
7. H. C. van de Hulst and R. Stark, "Accurate eigenvalues and exact extrapolation lengths in radiative transfer," Astron. Astrophys. **235**, 511–520 (1990).
8. E. Akkermans, P. E. Wolf, and R. Maynard, "Coherent backscattering of light by disordered media: analysis of the peak line shape," Phys. Rev. Lett. **56**, 1471–1474 (1986).
9. P.-E. Wolf and G. Maret, "Weak localization and coherent backscattering of photons in disordered media," Phys. Rev. Lett. **55**, 2696–2699 (1985).
10. M. P. V. Albada and A. Lagendijk, "Observation of weak localization of light in a random medium," Phys. Rev. Lett. **55**, 2692–2695 (1985).
11. M. B. van der Mark, M. P. van Albada, and A. Lagendijk, "Light scattering in strongly scattering media: multiple scattering and weak localization," Phys. Rev. B **37**, 3575–3592 (1988).
12. G. Labeyrie, F. de Tomasi, J.-C. Bernard, C. A. Müller, C. Miniatura, and R. Kaiser, "Coherent backscattering of light by cold atoms," Phys. Rev. Lett. **83**, 5266–5269 (1999).
13. Y. Bidel, B. Klappauf, J. C. Bernard, D. Delande, G. Labeyrie, C. Miniatura, D. Wilkowski, and R. Kaiser, "Coherent light transport in a cold strontium cloud," Phys. Rev. Lett. **88**, 203902 (2002).
14. G. Labeyrie, D. Delande, C. A. Müller, C. Miniatura, and R. Kaiser, "Coherent backscattering of light by an inhomogeneous cloud of cold atoms," Phys. Rev. A **67**, 033814 (2003).
15. O. Morice, Y. Castin, and J. Dalibard, "Refractive index of a dilute bose gas," Phys. Rev. A **51**, 3896–3901 (1995).
16. A. A. Svidzinsky, J.-T. Chang, and M. O. Scully, "Cooperative spontaneous emission of n atoms: many-body eigenstates, the effect of virtual lamb shift processes, and analogy with radiation of n classical oscillators," Phys. Rev. A **81**, 053821 (2010).
17. P. W. Courteille, S. Bux, E. Lucioni, K. Lauber, T. Bienaimé, R. Kaiser, and N. Piovella, "Modification of radiation pressure due to cooperative scattering of light," Eur. Phys. J. D **58**, 69–73 (2010).
18. T. Bienaimé, M. Petruzzo, D. Bigerni, N. Piovella, and R. Kaiser, "Atom and photon measurement in cooperative scattering by cold atoms," J. Mod. Opt. **58**, 1942–1950 (2011).
19. R. Bachelard, N. Piovella, and P. W. Courteille, "Cooperative scattering and radiation pressure force in dense atomic clouds," Phys. Rev. A **84**, 013821 (2011).
20. T. Bienaimé, S. Bux, E. Lucioni, P. W. Courteille, N. Piovella, and R. Kaiser, "Observation of a cooperative radiation force in the presence of disorder," Phys. Rev. Lett. **104**, 183602 (2010).
21. H. Bender, C. Stehle, S. Slama, R. Kaiser, N. Piovella, C. Zimmermann, and P. W. Courteille, "Observation of cooperative mie scattering from an ultracold atomic cloud," Phys. Rev. A **82**, 011404 (2010).
22. T. Bienaimé, R. Bachelard, J. Chabé, M. T. Rouabah, L. Bellando, P. W. Courteille, N. Piovella, and R. Kaiser, "Interplay between radiation pressure force and scattered light intensity in the cooperative scattering by cold atoms," J. Mod. Opt. **61**, 18–24 (2014).
23. I. M. Sokolov, M. D. Kupriyanova, D. V. Kupriyanov, and M. D. Havey, "Light scattering from a dense and ultracold atomic gas," Phys. Rev. A **79**, 053405 (2009).
24. T. M. Nieuwenhuizen, A. Lagendijk, and B. A. van Tiggelen, "Resonant point scatterers in multiple scattering of classical waves," Phys. Lett. A **169**, 191–194 (1992).
25. R. Bachelard, P. W. Courteille, R. Kaiser, and N. Piovella, "Resonances in Mie scattering by an inhomogeneous atomic cloud," EPL **97**, 14004 (2012).
26. R. Friedberg, S. Hartmann, and J. Manassah, "Frequency shifts in emission and absorption by resonant systems ot two-level atoms," Phys. Rep. **7**, 101–179 (1973).
27. J. T. Manassah, "Cooperative radiation from atoms in different geometries: decay rate and frequency shift," Adv. Opt. Photon. **4**, 108–156 (2012).
28. V. N. Fadeeva, *Computational Methods of Linear Algebra* (Dover, 1959).
29. S. B. Singham and C. F. Bohren, "Light scattering by an arbitrary particle: the scattering-order formulation of the coupled-dipole method," J. Opt. Soc. Am. A **5**, 1867–1872 (1988).
30. A. Goetschy and S. E. Skipetrov, "Non-Hermitian Euclidean random matrix theory," Phys. Rev. E **84**, 011150 (2011).
31. E. Akkermans, A. Gero, and R. Kaiser, "Photon localization and dicke superradiance in atomic gases," Phys. Rev. Lett. **101**, 103602 (2008).
32. S. E. Skipetrov and A. Goetschy, "Eigenvalue distributions of large euclidean random matrices for waves in random media," J. Phys. A **44**, 065102 (2011).
33. M. O. Scully, E. S. Fry, C. H. R. Ooi, and K. Wódkiewicz, "Directed spontaneous emission from an extended ensemble of n atoms: timing is everything," Phys. Rev. Lett. **96**, 010501 (2006).
34. A. A. Svidzinsky, J.-T. Chang, and M. O. Scully, "Dynamical evolution of correlated spontaneous emission of a single photon from a uniformly excited cloud of n atoms," Phys. Rev. Lett. **100**, 160504 (2008).
35. T. Karpiuk, N. Cherroret, K. L. Lee, B. Grémaud, C. A. Müller, and C. Miniatura, "Coherent forward scattering peak induced by anderson localization," Phys. Rev. Lett. **109**, 190601 (2012).
36. B. A. van Tiggelen, A. Lagendijk, and A. Tip, "Multiple-scattering effects for the propagation of light in 3D slabs," J. Phys. Condens. Matter **2**, 7653–7677 (1990).